A control-oriented model of underwater snake robots exposed to currents

A. M. Kohl*, E. Kelasidi*, K. Y. Pettersen* and J. T. Gravdahl†

***Abstract*— This paper presents a control-oriented model of a neutrally buoyant underwater snake robot that is exposed to a constant irrotational current. The robot is assumed to move in a horizontal, fully submerged plane with a sinusoidal gait pattern and limited link angles. The intention behind the proposed model is to describe the qualitative behaviour of the robot by a simplified kinematic approach, thus neglecting some of the non-linear effects that do not significantly contribute to the overall behaviour. This results in a model with significantly less complex dynamic equations than existing models, which makes the new model well-fitted for control design and analysis. An existing, more complex model and a class of sinusoidal gait patterns are analysed, leading to several properties that serve as a basis for the simplified model. Some of the revealed properties are also valid for ground robots. Simulations that qualitatively validate the theoretical results are presented.**

I. Introduction

A higher level of autonomy is desired in underwater operations such as underwater exploration, monitoring, surveillance and inspection. For ground applications, robots inspired by biological snakes have been shown to be especially well-suited for applications in irregular environments [1,2]. Motivated by this, amphibious and underwater snake robots (USRs) have been studied recently. They are considered promising to improve the autonomy, efficiency, and maneuverability of next generation underwater vehicles [3].

A basis for the development of USRs was formed by Gray, who studied the locomotion mechanisms of both fish [4] and snakes [5]. Later, Hirose proposed mathematical relationships describing snake motion, and developed the first snake robot prototypes [2]. For USRs, several mathematical models have been developed [3,6–10]. Most of these models are too complex to provide a basis for efficient control algorithms [7,8] or trade simplicity for a strongly simplified model of the fluid forces [6]. A model of a USR that considers both linear and non-linear drag effects, added mass effects and the presence of constant irrotational currents has been presented in [3]. The model is based on analytical fluid dynamics and a closed form of the dynamic equations is derived. This makes the model especially useful for control system purposes since it avoids iterative solutions of the fluid equations in each time step. However, due to the high complexity of the fluid dynamical model, the equations are still very complicated and make an analysis from a control systems theoretical point of view quite difficult. A simplified, control-oriented modelling approach that captures the overall, qualitative behaviour of the robot is therefore required. A first step towards such a simplified model for the special case with zero current was taken in [11], similar to a control-oriented model for ground snakes robot, that was first proposed in [12]. The control-oriented model is developed for undulating gait patterns, such as lateral undulation and eel-like motion, and is based on an assumption of small link angles.

This paper has several contributions. The first contribution is the analysis of the propulsive forces of an existing complex model of a USR exposed to current. It is an extension of the analysis in [11], where the special case with zero current has been studied. The analysis in this paper is carried out for the general case of a USR at first, and than narrowed down to the special case of sinusoidal motion patterns. The second contribution of this paper is twofold. The control-oriented model that was presented in [11] is generalised in order to consider constant irrotational currents, and in order to be applicable to a larger class of USRs. In previous studies, the control-oriented modelling approach has been restricted to robots whose fluid dynamical drag parameters had special properties. This restriction also occurred for ground robots, which can be regarded as a special case where the drag parameters are replaced by viscous friction coefficients. The results of this paper contribute thus also to the modelling of ground snake robots. As a third contribution, the gait pattern lateral undulation is analysed. For lateral undulation, the joints of the USR are controlled to move with a certain amplitude, which differs for the complex and the control-oriented model. In previous studies [1,11,12], these amplitudes have been found by trial and error. In this paper, however, analytical expressions are derived for the amplitudes of both models. The results are not restricted to underwater applications, but are also valid for ground robots with the same kinematics.

The paper is organised as follows. Sec. II briefly presents a model of USRs that has been derived in [3] based on analytical fluid dynamics. Additionally, the model is analysed so it can serve as a basis for the simplified model that is derived in Sec. III. In Sec. IV, the gait pattern lateral undulation is analysed and analytical expressions for the joint amplitude of both models are derived. Simulation results are given in Sec. V and conclusions and future work are presented in Sec. VI.

*Centre for Autonomous Marine Operations and Systems (AMOS), Department of Engineering Cybernetics at NTNU, NO-7491 Trondheim, Norway. E-mail: {Anna.Kohl,Eleni.Kelasidi,Kristin.Y.Pettersen}@itk.ntnu.no

†Department of Engineering Cybernetics at NTNU, NO-7491 Trondheim, Norway. E-mail: Tommy.Gravdahl@itk.ntnu.no

This work was partly supported by the Research Council of Norway through its Centres of Excellence funding scheme, project no. 223254-AMOS.

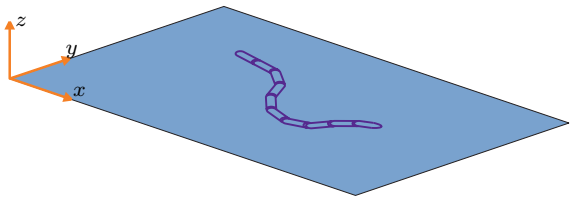

Fig. 1. The snake robot moving in a virtual horizontal plane

II. A FIRST-PRINCIPLE MODEL OF A USR

This section begins with a brief description of the dynamic model of a USR that was proposed in [3]. The kinematics of the model and its equations of motion are presented in Secs. II-A and II-B, respectively. The section is concluded by Sec. II-C, where the presented model is analysed as a basis for the simplified model that will be developed in Sec. III.

A. Kinematics

The robot is assumed to consist of N rigid links of length $2l$ each. The links are interconnected with $N-1$ active revolute joints. All links have the mass m, moment of inertia J, and uniform density, i.e. the center of mass (CM) is the center of geometry and the center of bouyancy.

The robot moves in a virtual horizontal plane and is fully submerged in water, as depicted in Fig. 1. It therefore has $N+2$ degrees of freedom, N corresponding to the orientation of each link, and two to the position of the CM on the virtual plane, denoted by $\begin{bmatrix} p_x & p_y \end{bmatrix} \in \mathbb{R}^2$. The orientation of each link $i \in 1, \cdots N$ w.r.t. the global x-axis is defined by the link angle θ_i. The orientation of the robot is defined as the average link angle $\bar{\theta} = \frac{1}{N}\sum_{i=1}^{N} \theta_i$. The relative angles between the single links, the actuated joint angles, are given by

$$\phi_i = \theta_i - \theta_{i+1}, \quad i \in 1 \cdots N-1. \tag{1}$$

B. Equations of motion

The hydrodynamic force $\mathbf{f}_i \in \mathbb{R}^2$ acting on link i is

$$\mathbf{f}_i = -\mathbf{F}^{\mathrm{a}}(\theta_i)\begin{bmatrix}\ddot{x}_i \\ \ddot{y}_i\end{bmatrix} + \mathbf{F}^{\mathrm{a,r}}(\theta_i,\dot{\theta}_i)\begin{bmatrix}V_x \\ V_y\end{bmatrix} - \mathbf{F}^{\mathrm{d}}(\theta_i)\begin{bmatrix}\dot{x}_i - V_x \\ \dot{y}_i - V_y\end{bmatrix} \tag{2}$$

in the global coordinate frame [3], with $\boldsymbol{v}_{\mathrm{c}} = \begin{bmatrix} V_x & V_y \end{bmatrix} \in \mathbb{R}^2$ denoting the current velocities in the inertial frame and

$$\begin{aligned}
\mathbf{F}^{\mathrm{a}}(\theta_i) &= \begin{bmatrix} \mu_n \sin^2\theta_i & -\mu_n \sin\theta_i\cos\theta_i \\ -\mu_n \sin\theta_i\cos\theta_i & \mu_n\cos^2\theta_i \end{bmatrix}, \\
\mathbf{F}^{\mathrm{a,r}}(\theta_i,\dot{\theta}_i) &= \begin{bmatrix} \mu_n \sin\theta_i\cos\theta_i\dot{\theta}_i & \mu_n \sin^2\theta_i\dot{\theta}_i \\ -\mu_n \cos^2\theta_i\dot{\theta}_i & -\mu_n \sin\theta_i\cos\theta_i\dot{\theta}_i \end{bmatrix}, \\
\mathbf{F}^{\mathrm{d}}(\theta_i) &= \begin{bmatrix} c_t\cos^2\theta_i + c_n\sin^2\theta_i & (c_t-c_n)\sin\theta_i\cos\theta_i \\ (c_t-c_n)\sin\theta_i\cos\theta_i & c_t\sin^2\theta_i + c_n\cos^2\theta_i \end{bmatrix}.
\end{aligned} \tag{3}$$

Here, the parameters μ_n, c_n, and c_t are the added mass parameter in the normal direction, and the drag parameters in the normal and tangential direction of the link, respectively. Details on their computation can be found in [3].

Assumption 1: The drag parameters of an underwater snake robot satisfy the anisotropic drag condition $c_n > c_t$.

Remark 1: Ass. 1 is valid because the drag parameters are functions of the fluid properties and the link geometry. The single links of the USR are modelled as elliptical cylinders, where the drag parameter in normal direction is typically larger than the one in tangential direction.

The fluid torque that acts on link i can be modelled by

$$\tau_i = -\lambda_1\ddot{\theta}_i - \lambda_2\dot{\theta}_i - \lambda_3\dot{\theta}_i|\dot{\theta}_i|. \tag{4}$$

The parameters λ_j depend on the link geometry and fluid properties [3].

Under the influence of the fluid forces and torques, the complete equations of motion of the USR are obtained as

$$\mathbf{M}_\theta\ddot{\boldsymbol{\theta}} + \mathbf{W}_\theta\dot{\boldsymbol{\theta}}^2 + \mathbf{V}_\theta\dot{\boldsymbol{\theta}} + \boldsymbol{\Lambda}_3\dot{\boldsymbol{\theta}}|\dot{\boldsymbol{\theta}}| + \mathbf{g}(\boldsymbol{\theta},\mathbf{f}_{\mathrm{d}}) = \mathbf{D}^T\mathbf{u}, \tag{5a}$$

$$Nm\ddot{p}_x = \sum_{i=1}^{N} f_{x,i}, \tag{5b}$$

$$Nm\ddot{p}_y = \sum_{i=1}^{N} f_{y,i}, \tag{5c}$$

with the drag forces $\mathbf{f}_{\mathrm{d}}$, a summation matrix $\mathbf{D}$, and the control input $\mathbf{u} \in \mathbb{R}^{N-1}$. For details and the derivation of the matrices $\mathbf{M}_\theta, \mathbf{W}_\theta, \mathbf{V}_\theta, \boldsymbol{\Lambda}_3$, and the function $\mathbf{g}$, see [3].

Remark 2: In the original model in [3], non-linear drag effects are considered additionally. It will turn out in the following sections of this paper that the control-oriented model is only capable of representing relatively slowly swimming robots. Therefore these effects, that only contribute to the fluid forces at high velocities, are neglected here.

C. Analysis of the complex model

1) Analysis of propulsive forces: As a preparation for the simplified model, this section investigates how a USR can achieve forward propulsion in the presence of a constant, irrotational current. At first, the fluid forces will be analysed generally, without assuming a certain motion pattern of the robot. In the second part, the special case of sinusoidal motion patterns will be investigated.

An analysis of the forces that move a ground snake robot was already introduced in [12]. For underwater snake robots described by (5), it was first proposed in [11]. In this paper, the analysis is generalised to robots that are exposed to currents. For the analysis, it is assumed without loss of generality that the forward direction of the USR is aligned with the global x-axis. The propulsive force is then the sum of all external forces in x-direction. It is obtained by inserting (2) into (5b):

$$\begin{aligned}
Nm\ddot{p}_x = &\underbrace{-\sum_{i=1}^{N} F_{11}^{\mathrm{a}}\ddot{x}_i}_{\mathrm{I}} \underbrace{-\sum_{i=1}^{N} F_{12}^{\mathrm{a}}\ddot{y}_i}_{\mathrm{II}} \underbrace{-\sum_{i=1}^{N} F_{11}^{\mathrm{d}}\dot{x}_i}_{\mathrm{III}} \underbrace{-\sum_{i=1}^{N} F_{12}^{\mathrm{d}}\dot{y}_i}_{\mathrm{IV}} \\
&\underbrace{+\sum_{i=1}^{N} F_{11}^{\mathrm{a,r}}V_x}_{\mathrm{V}} \underbrace{+\sum_{i=1}^{N} F_{12}^{\mathrm{a,r}}V_y}_{\mathrm{VI}} \underbrace{+\sum_{i=1}^{N} F_{11}^{\mathrm{d}}V_x}_{\mathrm{VII}} \underbrace{+\sum_{i=1}^{N} F_{12}^{\mathrm{d}}V_y}_{\mathrm{VIII}}
\end{aligned} \tag{6}$$

The function arguments (θ_i) and $(\theta_i,\dot{\theta}_i)$ have been omitted for better readability. Terms I-IV in (6) have already been analysed in [11] and the results will be summarised briefly here. Under the assumption that the forward velocities of the robot and each link are $\dot{x}_i > 0$, and the parameters μ_n, c_n, and c_t are positive, their properties are:

I: This term always opposes the acceleration of the link. It contributes to the propulsion when the link is slowing down, $\ddot{x}_i < 0$ and vice versa.

II: The expression $F_{12}^{\mathrm{a}}\ddot{y}_i$ is negative when $\mathrm{sgn}(\theta_i) = \mathrm{sgn}(\ddot{y}_i)$ and positive otherwise.

III: The product $F_{11}^{\mathrm{d}}\dot{x}_i$ is always positive, i.e. term III opposes the forward motion. This is the fluid drag force.

IV: The term $F_{12}^{\mathrm{d}}\dot{y}_i$ is negative when $\mathrm{sgn}(\theta_i) = \mathrm{sgn}(\dot{y}_i)$.

Compared to previous studies, terms V-VIII have to be considered additionally when a current is taken into account:

V: The product $F_{11}^{\mathrm{a,r}}V_x = \mu_n \sin\theta_i \cos\theta_i \dot{\theta}_i V_x$ has the same sign as V_x when $\mathrm{sgn}(\theta_i) = \mathrm{sgn}(\dot{\theta}_i), |\theta_i| < \frac{\pi}{2}$. This can be concluded from the fact that $\sin\theta_i \cos\theta_i > 0$ for $0 < \theta_i < \frac{\pi}{2}$ and $\sin\theta_i \cos\theta_i < 0$ for $0 > \theta_i > -\frac{\pi}{2}$.

VI: The expression $F_{12}^{\mathrm{a,r}}V_y = \mu_n \sin^2\theta_i \dot{\theta}_i V_y$ has the same sign as V_y when $\dot{\theta}_i > 0$ and the opposite when $\dot{\theta}_i < 0$.

VII: The sign of this term is always determined by V_x, since $F_{11}^{\mathrm{d}}V_x = (c_t \cos^2\theta_i + c_n \sin^2\theta_i)V_x$. This term causes the robot to flow with the current when the joints are not actuated.

VIII: For $F_{12}^{\mathrm{d}}V_y = (c_t - c_n)\sin\theta_i \cos\theta_i V_y$, the property $\mathrm{sgn}(F_{12}^{\mathrm{d}}) = -\mathrm{sgn}(\theta_i)$ holds for $|\theta_i| < \frac{\pi}{2}$, because $c_t < c_n$.

So far, these properties are general and not dependent on the gait pattern. It turns out that for a certain motion pattern, some simplifications are possible. This motion pattern can be described by a sinusoidal wave, that is propagated through the body from head to tail. The motion pattern will be explained and analysed in detail in Sec. IV. For the analysis in the next paragraph, it is sufficient to assume that the body-shape of the robot can be described by a propagating wave.

Assumption 2: An underwater snake robot is assumed to move forwards with a sinusoidal gait pattern. The phase offset between the links is chosen as $\delta = \frac{2\pi}{N-1}$, such that the period of the gait pattern equals the length of the USR. It was pointed out in [13] that this choice of period is beneficial for the efficiency of the propulsion for robots moving in corridor-like environments.

The influence of the single terms on the forward propulsion of the USR under Ass. 2 is summarized in the following: Term I always opposes the acceleration of the link $\ddot{x}_i$ and its magnitude scales with $\ddot{x}_i$. In a sinus wave propagating in x-direction, these accelerations are very small, and term I will not have a large impact. Most of the remaining terms in (6) cancel each other when the sums $\sum_{i=1}^{N}$ are evaluated. The cancellations are visualised in Fig. 2. The arrows indicate in which direction the resulting force points for each of the terms II - VIII, under the assumption that both $V_x, V_y > 0$. Due to the symmetry of the sinusoidal shape, terms with arrows in both directions cancel each other when the sum $\sum_{i=1}^{N}$ is computed. In the case that $V_x < 0$ (resp. $V_y < 0$), the arrows in terms V, VII (resp. terms VI, VIII) point in the opposite direction. The resulting forces in terms V,VI and VIII still cancel each other when summed up, while term VII, whose sign depends on the direction of the current, has an effect in the negative direction. The remaining terms in Fig. 2 are terms III and IV, which are the drag force and the main propulsive force, respectively. The result of the previous analysis is summarised in the following property.

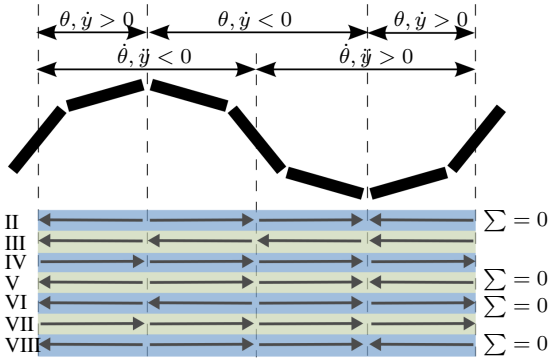

Fig. 2. Cancellation of the force

Property 1 (Main propulsive forces): For a USR that fulfils Ass. 1 and 2, term IV is the only term that causes forward propulsion independently of the current. Term I is not significant, and the remaining terms cancel each other except from the drag force in term III, always opposing the forward motion, and the effect of the current component in term VII, acting in the same direction as V_x.

From [1] and [11] we obtain a second important property:

Property 2 (Forward propulsion): For a snake robot with $c_n > c_t$, forward propulsion is mainly achieved by the transversal motion of the link.

Remark 3: In the previous analysis it has been assumed that the length of the USR equals the undulation period and the wave propagates with a constant amplitude. Even when these assumptions are slightly relaxed, the parts of terms II, V, VI, and VIII that have a counterpart will still cancel each other. It is thus a valid assumption that the robot satisfies Prop. 1, and the remaining resulting forces can be considered as small disturbances.

2) Analysis of turning locomotion and link motion: A detailed analysis of the turning behaviour of the robot and the link motion during lateral undulation has already been presented in [11]. The results match well with the corresponding analyses of the ground robot model in [12]. The presence of current does not play a role in these analyses, so the results from [11] will simply be summarized here.

Property 3 (Turning locomotion): During lateral undulation of a USR described by (5), the direction of motion is constant when the average joint angle is zero, i.e. $\phi_0 = 0$. The robot will turn (counter-)clockwise when the average joint angle is positive (negative). The turning rate will increase with an increase of the average joint angle and/or the forward velocity.

Property 4 (Link motion): The link motion of a USR according to (5) consists mainly of a normal displacement of the CM of each link w.r.t. the direction of motion.

III. A CONTROL-ORIENTED MODEL OF A USR

In this section a simplified model of a lateral undulating USR, developed for analysis and control design purposes, is presented. The approach was first proposed for a control-oriented dynamic model of ground robots in [12] and, for

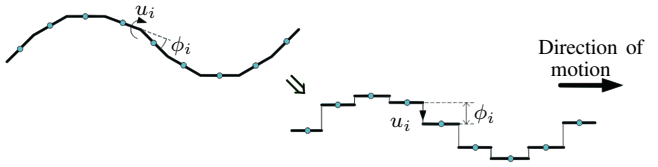

Fig. 3. Modelling of the revolute joints as prismatic joints [12]

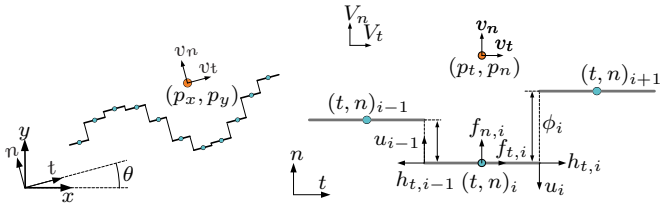

(a) The coordinate frames (b) Kinematics and dynamics

Fig. 4. The control-oriented model [12]

the simple case with no current, for USRs in [11]. Based on this, a more general model is developed in this paper. The new model is valid in the presence of current and for a larger class of robots. Its applications include both land-based, amphibious, and swimming snake robots.

A. Modelling approach and kinematics

In order to derive the control-oriented model, the revolute joints of the robot are modelled as prismatic joints, with their degree of freedom normal to the direction of motion of the robot, as visualized in Fig. 3. This is a strong simplification, but still a valid approximation, keeping in mind that according to Props. 2 and 4, the links move mainly in normal direction, which is also responsible for forward propulsion.

For the kinematics and dynamical equations of the robot, the following notation is used: The unity matrix $\mathbf{I}_N \in \mathbb{R}^{N\times N}$,

$$\mathbf{A} = \begin{bmatrix} 1 & 1 & & \\ & \ddots & \ddots & \\ & & 1 & 1 \end{bmatrix}, \qquad \mathbf{D} = \begin{bmatrix} 1 & -1 & & \\ & \ddots & \ddots & \\ & & 1 & -1 \end{bmatrix},$$

with $\mathbf{A}, \mathbf{D} \in \mathbb{R}^{(N-1)\times N}$. In addition, the summation vectors $\mathbf{e} = \begin{bmatrix} 1 & \dots & 1 \end{bmatrix}^T \in \mathbb{R}^N, \bar{\mathbf{e}} = \begin{bmatrix} 1 & \dots & 1 \end{bmatrix}^T \in \mathbb{R}^{N-1}$, and the pseudo-inverse $\bar{\mathbf{D}} = \mathbf{D}^T \left(\mathbf{D}\mathbf{D}^T\right)^{-1} \in \mathbb{R}^{N\times(N-1)}$ are defined.

The USR is assumed to undulate in a virtual horizontal plane. Just like the complex model, it consists of N links of length $L = 2l$ and mass m, that are connected by $N-1$ joints, which now have one translational degree of freedom each. The robot thus has $N+2$ degrees of freedom, two corresponding to the position in the plane, $N-1$ corresponding to the joint coordinates ϕ_i, and one to the orientation θ. Since the single links do not rotate w.r.t. each other, they all have the same orientation θ, which also defines the orientation of the robot.

For the description of the USR, two coordinate frames are introduced: the global x-y-frame, and the body-aligned t-n-frame. The origins of both frames coincide, as can be seen in Fig. 4(a). The dynamics of the simplified model is visualised in Fig. 4(b). The joint coordinates ϕ_i are no longer rotational, but prismatic and controlled by the input $\mathbf{u} \in \mathbb{R}^{N-1}$.

The following paragraph introduces the most important kinematic equations of the control-oriented model. They have originally been derived for a ground robot in [12], and later shown to be valid for USRs in [11]. Since they are a basis for the derivation of the simplified model with currents effect in the following, they will be shortly summarised here. For more details the reader is referred to the literature [1,11,12].

In [1,12], the relationship between the x-y-frame velocities and the t-n-frame velocities of the CM is shown to be

$$\dot{p}_x = v_t \cos\theta - v_n \sin\theta, \quad \dot{p}_y = v_t \sin\theta + v_n \cos\theta. \tag{7}$$

The link positions can be expressed in vector form as

$$\mathbf{t} = p_t \mathbf{e} - l\bar{\mathbf{D}}\bar{\mathbf{e}}, \quad \mathbf{n} = p_n \mathbf{e} - \bar{\mathbf{D}}\boldsymbol{\phi}, \tag{8}$$

and the link velocities as

$$\dot{\mathbf{t}} = (v_t + p_n\dot{\theta})\mathbf{e}, \quad \dot{\mathbf{n}} = (v_n - p_t\dot{\theta})\mathbf{e} - \bar{\mathbf{D}}\dot{\boldsymbol{\phi}}. \tag{9}$$

The corresponding link accelerations are given as [11]:

$$\ddot{\mathbf{t}} = (\dot{v}_t + \dot{p}_n\dot{\theta} + p_n\ddot{\theta})\mathbf{e}, \quad \ddot{\mathbf{n}} = (\dot{v}_n - \dot{p}_t\dot{\theta} - p_t\ddot{\theta})\mathbf{e} - \bar{\mathbf{D}}\ddot{\boldsymbol{\phi}}. \tag{10}$$

B. Fluid dynamic model

For the derivation of the fluid dynamical model, two basic assumptions are made in [11] and [1]:

Assumption 3 ([11]): The angluar velocity $\dot{\theta}_i \approx 0$ and its derivative $\ddot{\theta}_i \approx 0$ are assumed to be zero because the angular motion of the USR is much slower than the body shape dynamics.

As far as the propulsive force goes, Ass. 3 is additionally supported by the analysis in Sec. II-C.1, where it is shown that the terms containing $\dot{\theta}_i$ do not have an impact on the propulsion of the robot.

Assumption 4 ([1]): The link angles θ_i are assumed to be small. Furthermore, for $|\theta_i| < 20°$, the following approximations are made: $\sin^2\theta_i \approx 0, \cos^2\theta_i \approx 1, \sin\theta_i\cos\theta_i \approx \theta_i$. According to Ass. 4, the term $F_{11}^{\mathrm{d}} = c_t\cos^2\theta_i + c_n\sin^2\theta_i \approx c_t$. It has already been pointed out in [1], however, that the quality of this approximation depends on the ratio of the friction coefficients $\frac{c_n}{c_t}$. In the case of ground robots studied in [1], this ratio can be chosen to be sufficiently small for the assumption to hold. For underwater robots, however, the drag parameters c_n, c_t cannot be chosen independently from each other and their ratio will typically be $\mathcal{O}(c_n) \approx 10\mathcal{O}(c_t)$. The sine term in F_{11}^{d} is weighted by the larger coefficient c_n and therefore has to be taken into account in the modelling. This is an important insight, because for an efficient propulsion of a snake robot, a high $\frac{c_n}{c_t}$ ratio is advantageous, also for ground robots. By taking into account the term $c_n\sin^2\theta_i$, the control-oriented modelling approach becomes capable of describing robots with this desired property. Ass. 4 will therefore be reformulated in the following, making use of the common approximation $\sin\theta_i \approx \theta_i$ for small angles θ_i.

Assumption 5: The link angles θ_i are assumed to be small. Furthermore, for $|\theta_i| < 20°$, the following approximations are made: $\sin\theta_i \approx \theta_i$, $\sin^2\theta_i \approx 0$, $\cos^2\theta_i \approx 1$, $\sin\theta_i\cos\theta_i \approx \theta_i$, and $c_t\cos^2\theta_i + c_n\sin^2\theta_i \approx c_t + c_n\theta_i^2$.

In the terms F_{11}^{a} and F_{22}^{d}, the $\sin^2\theta_i$ is not multiplied with the large factor c_n and has no considerable effect. It can thus still be approximated by 0 in the control-oriented model where the goal is to model the significant effects while keeping the model as simple as possible for design and analysis purposes.

Remark 4: Note that for the control-oriented approach presented in [11], different values were considered for the drag parameters in the complex and the simplified model in order to circumvent the restriction on $\frac{c_n}{c_t}$. However, with Ass. 5, we are able to use the same values for the drag parameters for both the complex and the simplified model in this paper.

Equipped with Ass. 3 and 5, the fluid forces (2) simplify:

$$\begin{aligned}\begin{bmatrix} f_{x,i} \\ f_{y,i} \end{bmatrix} = &- \begin{bmatrix} 0 & -\mu_n\theta_i \\ -\mu_n\theta_i & \mu_n \end{bmatrix} \begin{bmatrix} \ddot{x}_i \\ \ddot{y}_i \end{bmatrix} \\ &- \begin{bmatrix} c_t + c_n\theta_i^2 & (c_t - c_n)\theta_i \\ (c_t - c_n)\theta_i & c_n \end{bmatrix} \begin{bmatrix} \dot{x}_i - V_x \\ \dot{y}_i - V_y \end{bmatrix}.\end{aligned} \tag{11}$$

Since the orientation of the single links θ_i is not captured by the control-oriented model, it has to be approximated. It is shown in [1] that the link angles can be estimated by

$$\theta_i \approx \frac{y_{i+1} - y_{i-1}}{2l} = \frac{\phi_{i-1} + \phi_i}{2l}. \tag{12}$$

Because the robot is assumed to be aligned with the global x-axis, Eqs. (8), (9) can be inserted into (11). With Eq. (12) and Ass. 3 that $\dot{\theta}_i, \ddot{\theta}_i \approx 0$, the forces simplify to

$$\begin{aligned}\begin{bmatrix} f_{t,i} \\ f_{n,i} \end{bmatrix} = &\begin{bmatrix} 0 & \mu_p(\phi_{i-1} + \phi_i) \\ \mu_p(\phi_{i-1} + \phi_i) & -\mu_n \end{bmatrix} \begin{bmatrix} \ddot{t}_i \\ \ddot{n}_i \end{bmatrix} \\ - &\begin{bmatrix} c_t + \widehat{c}_n(\phi_{i-1} + \phi_i)^2 & c_p(\phi_{i-1} + \phi_i) \\ c_p(\phi_{i-1} + \phi_i) & c_n \end{bmatrix} \begin{bmatrix} \dot{t}_i - V_t \\ \dot{n}_i - V_n \end{bmatrix}\end{aligned} \tag{13}$$

in the t-n frame. The new parameters in (13) are defined as $c_p = \frac{c_n - c_t}{2l}, \mu_p = \frac{\mu_n}{2l}, \widehat{c}_n = \frac{c_n}{4l^2}$ and $\begin{bmatrix} V_t & V_n \end{bmatrix}^T \in \mathbb{R}^2$ is the current in the body-aligned frame.

When the equations for each of the links are put together in matrix form, the final form is

$$\begin{aligned}\mathbf{f}_t = &\mu_p \mathrm{diag}(\mathbf{A}^T\boldsymbol{\phi})(\dot{v}_n\mathbf{e} - \bar{\mathbf{D}}\ddot{\boldsymbol{\phi}}) + c_p\mathrm{diag}(\mathbf{A}^T\boldsymbol{\phi}) \\ &(v_{n,\mathrm{rel}}\mathbf{e} - \bar{\mathbf{D}}\dot{\boldsymbol{\phi}}) - \left[c_t\mathbf{I}_N + \widehat{c}_n\mathrm{diag}^2(\mathbf{A}^T\boldsymbol{\phi})\right] v_{t,\mathrm{rel}}\mathbf{e},\end{aligned} \tag{14a}$$

$$\begin{aligned}\mathbf{f}_n = &\mu_p\mathrm{diag}(\mathbf{A}^T\boldsymbol{\phi})\dot{v}_t\mathbf{e} - \mu_n(\dot{v}_n\mathbf{e} - \bar{\mathbf{D}}\ddot{\boldsymbol{\phi}}) \\ &+ c_p\mathrm{diag}(\mathbf{A}^T\boldsymbol{\phi})v_{t,\mathrm{rel}}\mathbf{e} - c_n(v_{n,\mathrm{rel}}\mathbf{e} - \bar{\mathbf{D}}\dot{\boldsymbol{\phi}}),\end{aligned} \tag{14b}$$

where the index $v_{.,\mathrm{rel}} = v_. - V_.$ denotes the relative velocity [14] and the $\mathrm{diag}(\cdot)$-operator assembles a diagonal matrix of the elements of its argument.

C. Equations of motion

1) Translational dynamics: According to [1], the dynamic equations for the translational dynamics of the control-oriented model are given as

$$\ddot{\boldsymbol{\phi}} = -\frac{1}{m}\mathbf{D}\mathbf{f}_n + \frac{1}{m}\mathbf{D}\mathbf{D}^T\mathbf{u}, \tag{15a}$$

$$\dot{v}_t = \frac{1}{Nm}\mathbf{e}^T\mathbf{f}_t, \tag{15b}$$

$$\dot{v}_n = \frac{1}{Nm}\mathbf{e}^T\mathbf{f}_n. \tag{15c}$$

In order to find the closed form, the fluid dynamical forces $\mathbf{f}_t(\dot{v}_n, \ddot{\boldsymbol{\phi}})$ and $\mathbf{f}_n(\dot{v}_t, \dot{v}_n, \ddot{\boldsymbol{\phi}})$ in (14) are inserted into (15). The equations of motion

$$\mathcal{M}(\boldsymbol{\phi})\ddot{\boldsymbol{\phi}} = -\mathcal{D}(\boldsymbol{\phi})\dot{\boldsymbol{\phi}} - \mathcal{K}(\boldsymbol{\phi}, \mathbf{v})\boldsymbol{\phi} + \mathbf{D}\mathbf{D}^T\mathbf{u}, \tag{16a}$$

$$\begin{aligned}\dot{v}_t = h_1(\boldsymbol{\phi})\Big[&\underbrace{2N\bar{\mathbf{e}}^T\boldsymbol{\phi}(c_p\widetilde{m} - c_n\mu_p)}_{h_2(\boldsymbol{\phi})} v_{n,\mathrm{rel}} \\ &+ \underbrace{\left(4c_p\mu_p(\bar{\mathbf{e}}^T\boldsymbol{\phi})^2 - N^2\widetilde{m}c_t - N\widetilde{m}\widehat{c}_n\mathbf{e}^T(\mathbf{A}^T\boldsymbol{\phi})^2\right)}_{h_3(\boldsymbol{\phi})} v_{t,\mathrm{rel}} \\ &- c_pN\widetilde{m}\boldsymbol{\phi}^T\mathbf{A}\bar{\mathbf{D}}\dot{\boldsymbol{\phi}} - \mu_pN\widetilde{m}\boldsymbol{\phi}^T\mathbf{A}\bar{\mathbf{D}}\ddot{\boldsymbol{\phi}}\Big],\end{aligned} \tag{16b}$$

$$\begin{aligned}\dot{v}_n = h_1(\boldsymbol{\phi})\Big[&\underbrace{\left(4c_p\mu_p(\bar{\mathbf{e}}^T\boldsymbol{\phi})^2 - N^2mc_n\right)}_{h_4(\boldsymbol{\phi})} v_{n,\mathrm{rel}} \\ &+ \underbrace{2\bar{\mathbf{e}}^T\boldsymbol{\phi}\big(Nc_pm - Nc_t\mu_p - \widehat{c}_n\mu_p\mathbf{e}^T(\mathbf{A}^T\boldsymbol{\phi})^2\big)}_{h_5(\boldsymbol{\phi})} v_{t,\mathrm{rel}} \\ &- 2c_p\mu_p\bar{\mathbf{e}}^T\boldsymbol{\phi}\boldsymbol{\phi}^T\mathbf{A}\bar{\mathbf{D}}\dot{\boldsymbol{\phi}} - 2\mu_p^2\bar{\mathbf{e}}^T\boldsymbol{\phi}\boldsymbol{\phi}^T\mathbf{A}\bar{\mathbf{D}}\ddot{\boldsymbol{\phi}}\Big]\end{aligned} \tag{16c}$$

can be derived, where $\widetilde{m} = m + \mu_n$. The function $h_1(\boldsymbol{\phi})$ is

$$h_1(\boldsymbol{\phi}) = \left[N^2m\widetilde{m} - 4\mu_p^2(\bar{\mathbf{e}}^T\boldsymbol{\phi})^2\right]^{-1} \tag{17}$$

and the matrices $\mathcal{M}(\boldsymbol{\phi}), \mathcal{D}(\boldsymbol{\phi}), \mathcal{K}(\boldsymbol{\phi}, \mathbf{v})$ are given by

$$\begin{aligned}\mathcal{M}(\boldsymbol{\phi}) &= \widetilde{m}\mathbf{I}_{N-1} + N\widetilde{m}\mu_p^2h_1(\boldsymbol{\phi})\mathbf{A}\mathbf{D}^T\boldsymbol{\phi}\boldsymbol{\phi}^T\mathbf{A}\bar{\mathbf{D}}, \\ \mathcal{D}(\boldsymbol{\phi}) &= c_n\mathbf{I}_{N-1} + N\widetilde{m}c_p\mu_ph_1(\boldsymbol{\phi})\mathbf{A}\mathbf{D}^T\boldsymbol{\phi}\boldsymbol{\phi}^T\mathbf{A}\bar{\mathbf{D}}, \\ \mathcal{K}(\boldsymbol{\phi}, \mathbf{v}) &= \mathbf{A}\mathbf{D}^T\Big(2N\mu_ph_1(\boldsymbol{\phi})\bar{\mathbf{e}}^T\boldsymbol{\phi}\big(c_n\mu_p - \widetilde{m}c_p\big)v_{n,\mathrm{rel}} \\ &\quad + N\widetilde{m}h_1(\boldsymbol{\phi})\big(N\mu_pc_t + \widehat{c}_n\mu_p\mathbf{e}^T(\mathbf{A}^T\boldsymbol{\phi})^2 - Nmc_p\big)v_{t,\mathrm{rel}}\Big).\end{aligned} \tag{18}$$

The operator $(\cdot)^2$ applied to a vector means that each of the vector's elements is squared.

2) Rotational dynamics: The rotational dynamics of the USR has already been derived in [11] for the special case of zero current:

$$\ddot{\theta} = \tfrac{1}{1+\lambda_3}\Big(-\lambda_1\dot{\theta} + \tfrac{\lambda_2}{N-1}v_t\bar{\mathbf{e}}^T\boldsymbol{\phi}\Big) \tag{19}$$

In order to take into account the current, the absolute velocity v_t has to be replaced by the relative velocity $v_{t,\mathrm{rel}}$ [14]:

$$\ddot{\theta} = -\widetilde{\lambda}_1\dot{\theta} + \tfrac{\widetilde{\lambda}_2}{N-1}v_{t,\mathrm{rel}}\bar{\mathbf{e}}^T\boldsymbol{\phi} \tag{20}$$

In (20), the coefficients were redefined as $\widetilde{\lambda}_1 := \lambda_1/(1+\lambda_3)$ and $\widetilde{\lambda}_2 := \lambda_2/(1+\lambda_3)$ in order to simplify the expression. The equation now has the same structure as the formulation that is given for the control-oriented ground model in [1], which it reduces to for the particular case of ground robots. In that case, the added mass and current effects are set to zero and the drag forces are replaced by viscous ground friction forces.

D. The complete control-oriented model

In order to describe the second order system with $N+2$ degrees of freedom, a state vector $\mathbf{x} \in \mathbb{R}^{2N+4}$ containing the generalised coordinates and velocities is required:

$$\mathbf{x} = \begin{bmatrix} \boldsymbol{\phi}^T & \theta & p_x & p_y & \mathbf{v}_\phi^T & v_\theta & v_t & v_n \end{bmatrix}^T \in \mathbb{R}^{2N+4}. \tag{21}$$

The linearising control law

$$\mathbf{u} = (\mathbf{D}\mathbf{D}^T)^{-1}\Big[\mathcal{M}(\boldsymbol{\phi})\bar{\mathbf{u}} + \mathcal{D}(\boldsymbol{\phi})\dot{\boldsymbol{\phi}} + \mathcal{K}(\boldsymbol{\phi}, \mathbf{v})\boldsymbol{\phi}\Big] \tag{22}$$

transforms the joint dynamics (16a) to $\ddot{\boldsymbol{\phi}} = \bar{\mathbf{u}}$ with the new input $\bar{\mathbf{u}} = \begin{bmatrix}\bar{u}_1 & \cdots & \bar{u}_{N-1}\end{bmatrix}^T \in \mathbb{R}^{N-1}$.

With the new control input, the accelerations (16) and (20), and the relation (7), the closed-loop control-oriented model of the underwater snake robot is then given by

$$\dot{\boldsymbol{\phi}} = \mathbf{v}_\phi, \tag{23a}$$
$$\dot{\theta} = v_\theta, \tag{23b}$$
$$\dot{p}_x = v_t \cos\theta - v_n \sin\theta, \tag{23c}$$
$$\dot{p}_y = v_t \sin\theta + v_n \cos\theta, \tag{23d}$$
$$\dot{\mathbf{v}}_\phi = \bar{\mathbf{u}}, \tag{23e}$$
$$\dot{v}_\theta = -\widetilde{\lambda}_1 v_\theta + \tfrac{\widetilde{\lambda}_2}{N-1} v_{t,\mathrm{rel}} \bar{\mathbf{e}}^T \boldsymbol{\phi}, \tag{23f}$$
$$\begin{aligned}\dot{v}_t = h_1(\boldsymbol{\phi})\Big[&h_2(\boldsymbol{\phi}) v_{n,\mathrm{rel}} + h_3(\boldsymbol{\phi}) v_{t,\mathrm{rel}} \\ &- c_p N \widetilde{m} \boldsymbol{\phi}^T \mathbf{A}\bar{\mathbf{D}}\mathbf{v}_\phi - \mu_p N \widetilde{m} \boldsymbol{\phi}^T \mathbf{A}\bar{\mathbf{D}}\bar{\mathbf{u}}\Big],\end{aligned} \tag{23g}$$
$$\begin{aligned}\dot{v}_n = h_1(\boldsymbol{\phi})\Big[&h_4(\boldsymbol{\phi}) v_{n,\mathrm{rel}} + h_5(\boldsymbol{\phi}) v_{t,\mathrm{rel}} \\ &- 2c_p\mu_p \bar{\mathbf{e}}^T \boldsymbol{\phi}\boldsymbol{\phi}^T \mathbf{A}\bar{\mathbf{D}}\mathbf{v}_\phi - 2\mu_p^2 \bar{\mathbf{e}}^T \boldsymbol{\phi}\boldsymbol{\phi}^T \mathbf{A}\bar{\mathbf{D}}\bar{\mathbf{u}}\Big].\end{aligned} \tag{23h}$$

IV. Sinusoidal gait patterns

This section introduces a gait pattern by which the control-oriented model explained in the previous section can achieve forward propulsion. The most common gait pattern of ground snakes is lateral undulation [1]. The control-oriented model that is presented in this paper is developed for sinusoidal gait patterns, including but not limited to lateral undulation.

In order to achieve a sinusoidal motion for the simplified model, a joint controller has to be designed, where the translational joints are controlled to oscillate with an amplitude a that is usually given in cm. In the first-principle model on the other hand, the joints are revolute and controlled to move with an amplitude α, which is an angle. In order for the control-oriented model to represent the behaviour of the complex model, a mapping $\alpha \mapsto a$ has to be found. In previous studies [1,11,12,15], this mapping has been found by trial and error. This paper presents a mathematical description of the mapping $\alpha \mapsto a$. This is achieved by analysing both $\alpha = \alpha(\theta_{i,\max})$ and $a = a(\theta_{i,\max})$, i.e. the geometric relations between the maximal link orientation angle, and the joint angle and the normal distance between the single links, respectively. The case for the complex model is investigated in Sec. IV-A, and the case for the simplified model in Sec. IV-B.

A. Lateral undulation with revolute joints

The gait pattern lateral undulation is mathematically described by the serpenoid curve [2]. In [1], it is pointed out that this curve can be discretely approximated by

$$\theta_i(t) = \theta_{\max} \sin\left(\Omega t + (i-1)\Delta\right), \tag{24}$$

where each link angle, θ_i, oscillates with the amplitude $\theta_{\max}$, angular frequency Ω, and a constant offset Δ compared to the previous link. It is furthermore shown that this gait pattern is achieved by controlling the joints to follow

$$\phi_{i,\mathrm{ref}} = \alpha \sin\left(\omega t + (i-1)\delta\right) + \phi_0. \tag{25}$$

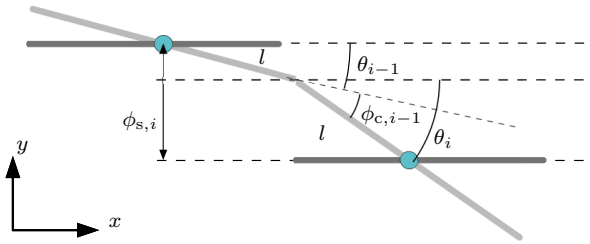

Fig. 5. The joint coordinates of the simplified model

By inserting (24) and (25) into (1), the desired function $\alpha = \alpha(\theta_{i,\max})$ is obtained:

$$\begin{aligned}\phi_i &= \theta_i - \theta_{i+1} \\ &= \theta_{\max}\sin\left(\Omega t + (i-1)\Delta\right) - \theta_{\max}\sin\left(\Omega t + i\Delta\right) \\ &= 2\theta_{\max}\cos\left(\tfrac{2\Omega t + (i-1)\Delta + i\Delta}{2}\right)\sin\left(\tfrac{\Omega t + (i-1)\Delta - \Omega t - i\Delta}{2}\right) \\ &= -2\theta_{\max}\cos\left(\Omega t + (i-1)\Delta + \tfrac{\Delta}{2}\right)\sin\left(\tfrac{\Delta}{2}\right) \\ &= \underbrace{2\theta_{\max}\sin\tfrac{\Delta}{2}}_{=\phi_{\max}}\sin\Bigg(\Omega t + (i-1)\Delta + \underbrace{\tfrac{\Delta}{2} + \tfrac{3\pi}{2}}_{=\widehat{\delta}}\Bigg).\end{aligned} \tag{26}$$

This shows that the joint angles oscillate with the amplitude $\phi_{\max}$ and the same angular frequency $\omega = \Omega$ and the same constant offset $\delta = \Delta$ between each other like the link orientation. There is just a constant shift $\widehat{\delta}$ between the maximal joint and link angle.

Proposition 1: Let a snake robot described by the complex model (5) move with lateral undulation according to (24). Then, the amplitude of the joint angles is given by

$$\alpha = \phi_{\max} = 2\sin\left(\tfrac{\delta}{2}\right)\theta_{\max}. \tag{27}$$

Remark 5: The statement in Proposition 1 is not limited to underwater snake robots. It also holds true for ground robots when their kinematics can be described as in Sec. II-A.

B. Lateral undulation with translational joints

For the control-oriented model, the parameter that has to be found is the maximal normal distance between the single oscillating links, referred to as the joint distance ϕ_i. From the geometry of the robot, Fig. 5, it can be seen that

$$\phi_i = l\sin\theta_{i+1} + l\sin\theta_i. \tag{28}$$

In Fig. 5, ϕ_s and ϕ_c refer to the joint distance of the simplified model and the joint angle of the complex model, respectively.

When (24) is inserted into (28), the amplitude for the oscillation of the joint coordinates, a, can be determined:

$$\begin{aligned}\phi_i = l\sin\Big(\theta_{\max}\sin\big(\Omega t + i\Delta\big)\Big) \\ + l\sin\Big(\theta_{\max}\sin\big(\Omega t + (i-1)\Delta\big)\Big).\end{aligned} \tag{29}$$

From (29) it is clear that the motion of the joint coordinates is not described by a simple sine function, but by the composition of two sine functions. For small angles, however,

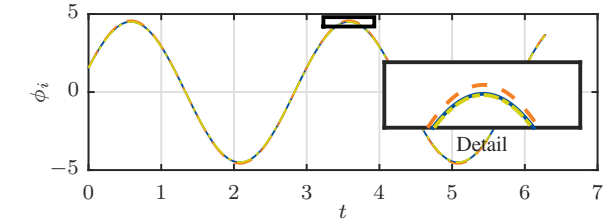

Eq. (28): $\phi_i = l\sin\theta_{i+1} + l\sin\theta_i$
Eq. (30): $\phi_i = l\theta_{\max}\big[\sin\big(\Omega t + i\Delta\big) + \sin\big(\Omega t + (i-1)\Delta\big)\big]$
Eq. (31): $\phi_i = l\sin\theta_{\max}\big[\sin\big(\Omega t + i\Delta\big) + \sin\big(\Omega t + (i-1)\Delta\big)\big]$

Fig. 6. The joint coordinates of link i over time

$\sin\theta_i \approx \theta_i$ according to Ass. 5, and (29) simplifies to

$$\phi_i \approx l\theta_{\max}\Big(\sin(\Omega t + i\Delta) + \sin(\Omega t + (i-1)\Delta)\Big). \quad (30)$$

Since the parameter we are looking to find is the amplitude of the oscillation, the approximation can be improved by taking into account the outer sine function in that amplitude:

$$\phi_i \approx l\sin\theta_{\max}\Big(\sin\big(\Omega t + i\Delta\big) + \sin\big(\Omega t + (i-1)\Delta\big)\Big). \quad (31)$$

This is verified by simulations. The amplitude ϕ_i of the joint angle for link i over time is plotted in Fig. 6 for the worst case, a maximal joint angle of $\theta_{\max} = 20°$. The plot clearly shows that both (30) and (31) are good approximations of (29), but that (31) represents the amplitude more accurately. The bracket term in (31) can analogously to (26) be summarized as follows:

$$\begin{aligned}\phi_i &= 2l\sin\theta_{\max}\sin\Big(\tfrac{2\Omega t + (i-1)\Delta + i\Delta}{2}\Big)\cos\big(\tfrac{\Delta}{2}\big) \quad (32)\\ &= \underbrace{2l\sin\theta_{\max}\cos\big(\tfrac{\Delta}{2}\big)}_{=\phi_{\max}}\sin\Big(\Omega t + (i-1)\Delta + \underbrace{\tfrac{\Delta}{2}}_{=\widehat{\delta}}\Big).\end{aligned}$$

Just like for the motion of the complex model we see that the angular frequency $\Omega = \omega$ and the offset between subsequent links $\Delta = \delta$ are the same, and a constant offset $\widehat{\delta} = \frac{\delta}{2}$ remains.

Proposition 2: Let a snake robot described by the simplified model (23) move with the gait pattern lateral undulation according to (24) and with a maximal link angle $|\theta_i| < 20°$. Then, the amplitude of the joint coordinates is given by

$$a = \phi_{\max} = 2l\cos\big(\tfrac{\delta}{2}\big)\sin\theta_{\max}. \quad (33)$$

V. Numerical Results

This section provides simulation results that show how the control-oriented model developed in Sec. III can be used to approximate the behaviour of the complex model that was presented in Sec. II. In the first part, the parameters that were chosen for the simulations are defined. In the second part, simulation results are shown for straight and turning motion.

A. Simulation parameters

Both models were implemented and simulated in *Matlab R2014b*. The dynamics of the models was calculated by the *ode23tb* solver in Matlab with a relative and absolute error tolerance of 10^{-4}. A snake robot with $N = 10$ links was considered, analogously to the example in [3]: Each of the links was modelled as a cylinder with major radius $a = 0.05\,\mathrm{m}$, minor radius $b = 0.03\,\mathrm{m}$, and length $2l = 0.14\,\mathrm{m}$. The mass of each link was assumed to be $m = 0.6597\,\mathrm{kg}$, in order to achieve neutral buoyancy. The fluid parameters are given by $c_n = 8.4$, $c_t = 0.2639$, $\mu_n = 0.3958$, $\lambda_1 = 2.2988 \cdot 10^{-7}$, $\lambda_2 = 4.3103 \cdot 10^{-4}$, and $\lambda_3 = 2.2629 \cdot 10^{-5}$. A constant irrotational current $\boldsymbol{v}_c = \big[0.1\frac{\mathrm{m}}{\mathrm{s}} \quad 0.1\frac{\mathrm{m}}{\mathrm{s}}\big]^T$ is assumed. The parameters for the rotational dynamics of the simplified model were determined as $\widetilde{\lambda}_1 = 1.15$ and $\widetilde{\lambda}_2 = 40$ by trial and error in order to achieve a good quantitative approximation. The initial values of both models were chosen as the origin.

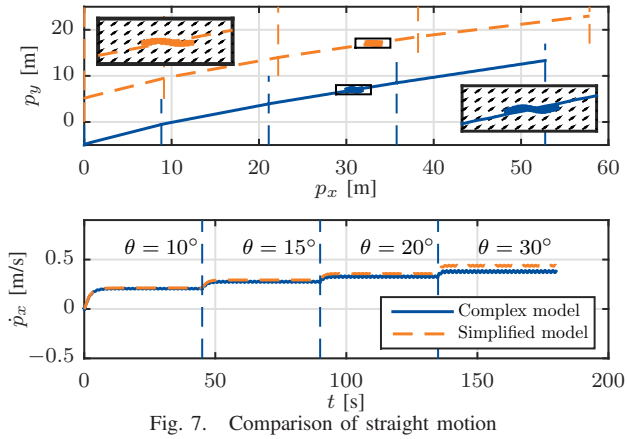

Fig. 7. Comparison of straight motion

For the control of the joint dynamics, a PD-controller was used for both the complex and the simplified model:

$$\bar{\mathbf{u}} = \ddot{\boldsymbol{\phi}}_{\mathrm{ref}} + k_d(\dot{\boldsymbol{\phi}}_{\mathrm{ref}} - \dot{\boldsymbol{\phi}}) + k_p(\boldsymbol{\phi}_{\mathrm{ref}} - \boldsymbol{\phi}) \quad (34)$$

where the control parameters are $k_p = 200$ and $k_d = 50$. The reference signal $\boldsymbol{\phi}_{\mathrm{ref}}$ is given by (25) and $\dot{\boldsymbol{\phi}}_{\mathrm{ref}}, \ddot{\boldsymbol{\phi}}_{\mathrm{ref}}$ are obtained from its time derivatives. The undulation parameters ω and δ were defined as $\omega = 120°, \delta = \frac{2\pi}{N-1} = 40°$. The parameters α resp. a, and ϕ_0 will be defined in the following.

B. Comparison of straight motion

In the first part of the simulation study both the complex and the simplified model were controlled with an open-loop controller to swim in a straight line. The initial values of the simulation were set according to Sec. V-A except for the position, where p_y was set to -5 for the complex model and to $+5$ for the simplified model, for better visibility. The joint offset ϕ_0 was set to zero during the whole simulation. In order to verify the mappings for the control amplitude that were derived in Sec. IV, the amplitude of the joint controller was increased every 45 seconds. The amplitudes were calculated from (27) and (33) corresponding to the maximal link angles $\theta_{\max} = 10°, 15°, 20°$, and $30°$, respectively.

The results of the simulation are depicted in Fig. 7. The first plot shows the position of the robots. The vertical lines indicate the position of each robot after 45 s, when the joint amplitude is increased. It can be seen that both models achieve forward motion in the x-direction and a drift in the y-direction due to the current component V_y. The second plot visualises the velocities in the x-direction over time. For the small link angles $\theta_{\max} = 10°, 15°$, a good accordance

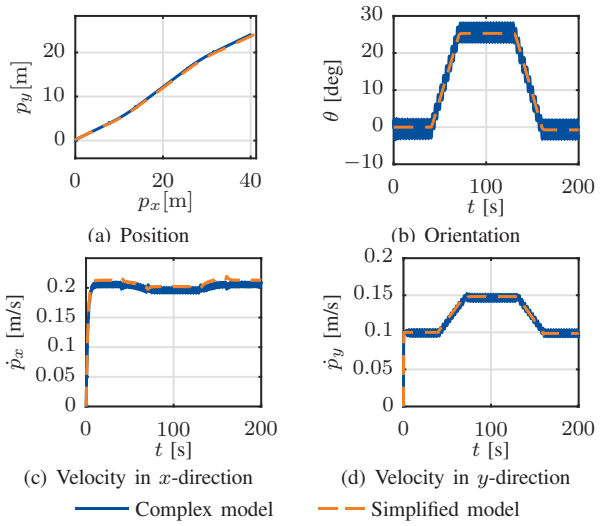

(a) Position (b) Orientation (c) Velocity in x-direction (d) Velocity in y-direction

Fig. 8. Comparison of turning motion

between the two models can be observed. For the larger angles, the simplified model overestimates the velocity of the complex one. This is a consequence of Ass. 5, which is only valid for $|\theta_i| < 20°$.

Fig. 7 shows the absolute velocity of the USR, not the relative. It can be seen that even for the largest simulated amplitude, the absolute velocity is smaller than $0.5\,\frac{\mathrm{m}}{\mathrm{s}}$. The relative velocity is even smaller than that, because the current has a positive x-component. This justifies the assumption in Rm. 2, that nonlinear drag effects in (2) can be neglected, because it becomes evident that the control-oriented model cannot be applied to high velocity scenarios.

C. Comparison of turning motion

In order to compare the model behaviour during turning motion, the following scenario was simulated: All initial conditions were chosen as described in Sec. V-A. The maximal link angle was assumed to be $\theta_{\max} = 10°$, and the amplitudes for the undulation were chosen as $\alpha = 6.84°$ and $a = 2.28\,\mathrm{cm}$, according to (27) and (33), respectively. The joint offset ϕ_0 was set to $\frac{\alpha}{6}, \frac{a}{6}$, respectively, in the time interval $t \in [40\,\mathrm{s}, 70\,\mathrm{s}]$, to $-\frac{\alpha}{6}, -\frac{a}{6}$ in $t \in [130\,\mathrm{s}, 160\,\mathrm{s}]$, and to zero elsewhere.

The results of the simulation can be seen in Fig. 8. In Fig. 8(a) the position of both models is given. It can be seen that a good qualitative and quantitative approximation is achieved. Fig. 8(b) depicts the orientation of both models over time. The simplified model neglects the higher order oscillations that are present for the complex model. Apart from that, a good accordance is observed. This has been achieved by a tuning of the parameters $\widetilde{\lambda}_1, \widetilde{\lambda}_2$. Figs. 8(c) and 8(d) show the velocity of the CM in the x- and y-direction, respectively. Obviously, the simplified model captures the mean velocities of the complex model quite well.

VI. Conclusions and Future Work

This paper has presented a control-oriented model of a fully submerged, neutrally buoyant USR exposed to a constant irrotational current, which was assumed to move in a horizontal plane with a sinusoidal gait pattern and small link angles. An existing, more complex model was analysed, leading to several properties that serve as a basis for the simplified model. Furthermore, the behaviour of that model during sinusoidal gait patterns was studied. Some of the revealed properties are also valid for ground robots. The control-oriented model was developed in order to qualitatively capture the behaviour of the complex model by a simplified kinematic approach, thus neglecting some of the non-linear effects that do not significantly contribute. This resulted in a model with significantly less complex dynamic equations, which makes it well-fitted for control design and analysis. Compared to previous studies, the control-oriented modelling approach was extended in order to be capable of modelling USRs with arbitrary drag parameters. In addition, analytical expressions for the amplitude of the joint controllers of both models were derived. Finally, simulations that qualitatively validate the theoretical results were presented. They show a good accordance between the two models as long as the link angles are sufficiently small.

In future work, the results will be generalized in order to also be applicable to eel-like motion. Furthermore, the model will be employed for analysis and control design for USRs.

References

[1] P. Liljebäck, K. Y. Pettersen, Ø. Stavdahl, and J. T. Gravdahl, *Snake Robots: Modelling, Mechatronics, and Control*, ser. Advances in Industrial Control. Springer London, 2012.

[2] S. Hirose, *Biologically Inspired Robots: Snake-Like Locomotors and Manipulators*. Oxford: Oxford University Press, 1993.

[3] E. Kelasidi, K. Y. Pettersen, J. T. Gravdahl, and P. Liljebäck, "Modeling of underwater snake robots," in *Proc. IEEE Int. Conf. Robotics and Automation*, Hong Kong, China, May, Jun. 2014.

[4] J. Gray, "Studies in animal locomotion I. the movement of fish with special reference to the eel," *J. Exp. Biol.*, vol. 10, no. 1, pp. 88–104, 1933.

[5] ——, "The mechanism of locomotion in snakes," *J. Exp. Biol.*, vol. 23, no. 2, pp. 101–120, 1946.

[6] K. Mclsaac and J. Ostrowski, "A geometric approach to anguilliform locomotion: modelling of an underwater eel robot," in *Proc. IEEE Int. Conf. Robotics and Automation*, Detroit, MI, May 1999.

[7] F. Boyer, M. Porez, and W. Khalil, "Macro-continuous computed torque algorithm for a three-dimensional eel-like robot," *IEEE Trans. Robot.*, vol. 22, no. 4, pp. 563–775, 2006.

[8] J. Blair and T. Iwasaki, "Optimal gaits for mechanical rectifier systems," *IEEE Trans. Autom. Control*, vol. 56, no. 1, pp. 59–71, 2011.

[9] A. J. Wiens and M. Nahon, "Optimally efficient swimming in hyper-redundant mechanisms: control, design, and energy recovery," *Bioinspiration & Biomimetics*, vol. 7, no. 4, 2012.

[10] M. Porez, F. Boyer, and A. J. Ijspeert, "Improved lighthill fish swimming model for bio-inspired robots: Modeling, computational aspects and experimental comparisons," *Int. J. Robot. Res.*, vol. 33, no. 10, pp. 1322–1341, 2014.

[11] E. Kelasidi, K. Y. Pettersen, and J. T. Gravdahl, "A control-oriented model of underwater snake robots," in *Proc. IEEE Int. Conf. Robotics and Biomimetics*, Bali, Indonesia, Dec. 2014.

[12] P. Liljebäck, K. Y. Pettersen, Ø. Stavdahl, and J. T. Gravdahl, "A simplified model of planar snake robot locomotion," in *Proc. IEEE/RSJ Int. Conf. Intelligent Robots and Systems*, Taipei, Taiwan, Oct. 2010.

[13] M. Sfakiotakis and D. P. Tsakiris, "Biomimetic centering for undulatory robots," *Int. J. Robot. Res.*, vol. 26, no. 11-12, pp. 1267–1282, 2007.

[14] T. I. Fossen, *Handbook of Marine Craft Hydrodynamics and Motion Control*. Wiley, 2011.

[15] E. Kelasidi, K. Y. Pettersen, and J. T. Gravdahl, "Stability analysis of underwater snake robot locomotion based on averaging theory," in *Proc. IEEE Int. Conf. Robotics and Biomimetics*, Bali, Indonesia, Dec. 2014.